Level scheme of ^{92}Nb and observation of an oblate collective rotational band

Zhen Ren [1], Jing-Bin Lu [1,*] Guo-Xiang Dong [2,†] Yun Zheng [3] Yi-Heng Wu [4] Tian-Jiao Gao [1] Pei-Yao Yang [1] Yan Hao [1] Ke-Yan Ma [1] Xiao-Guang Wu [3] Cong-Bo Li [3] Zhen Huang [5] Guang-Xin Zhang [6] Shi-Peng Hu [7] Hui-Bin Sun [8] Huan-Qiao Zhang [3] D. Testov [9,10] J. J. Valiente-Dobon [11] A. Goasduff [11] M. Siciliano [11,12] F. Galtarossa [11] D. Mengoni [9,10] D. Bazzacco [9,10] and Gao-Long Zhang [5,‡]

[1] *College of Physics, Jilin University, Changchun 130012, China*
[2] *School of Science, Huzhou University, Huzhou 313000, China*
[3] *China Institute of Atomic Energy, Beijing 102413, China*
[4] *School of Electronic Engineering and Intelligent Manufacturing, An Qing Normal University, Anqing 246133, China*
[5] *School of Physics, Beihang University, Beijing 100191, China*
[6] *Sino-French Institute of Nuclear Engineering and Technology, Sun Yat-sen University, Zhuhai 519082, Guangdong, China*
[7] *Institute for Advanced Study in Nuclear Energy and Safety, Shenzhen University, Shenzhen 518060, China*
[8] *College of Physics and Energy, Shenzhen University, Shenzhen 518060, China*
[9] *Dipartimento di Fisica Astronomia dell'Università di Padova, 35131 Padova, Italy*
[10] *Istituto Nazionale di Fisica Nucleare, Sezione di Padova, 35131 Padova, Italy*
[11] *INFN, Laboratori Nazionali di Legnaro, I-35020 Legnaro, Italy*
[12] *Physics Division, Argonne National Laboratory, Lemont, Illinois 60439, USA*

(Received 16 May 2023; revised 25 July 2023; accepted 22 September 2023; published 2 October 2023)

Excited states of ^{92}Nb were investigated using the reactions ^{82}Se(^{14}N, 4n) and ^{89}Y(^{6}Li, 1p2n). Based on these experimental results, the level scheme was extended abundantly. The structures of both the positive and negative parity states have been compared with shell model calculations using the SNET interaction. Potential energy surface calculation using the configuration-constrained method was performed to study a rotational-like band in ^{92}Nb, and possible configuration of the band head has been discussed. The calculation indicates that it may be an oblate collective rotational band.

DOI: 10.1103/PhysRevC.108.044301

I. INTRODUCTION

Nuclei near the $Z = 38$ subshell and the $N = 50$ closed shell are thought to be near-spherical and can be well described by the shell model [1–11]. Plenty of reactions were analyzed in this region and their level schemes have been extended to high excitation energies. Level structures of these nuclei are interpreted via single- or multiparticle excitations. Proton excitations play a vital role towards the generation of the low and moderate spin states. For the high spin states, the contribution of the proton $g_{9/2}$ orbit becomes essential and neutron excitations come into the picture to a suitable description of the nuclear structure.

Collective rotational structures have been reported in several nuclei in this region. A regular dipole band with enhanced $M1$ transitions was observed in ^{89}Zr and thought to represent rotation of nucleus about the long axis [12,13]. An oblate collective rotational band was discovered in ^{93}Nb [14]. These observations lead our interest to study the emergence of collectivity for nuclei near ^{90}Zr. To generate higher angular momentum, more particles are excited and high-j orbits such as the proton $g_{9/2}$ and neutron $h_{11/2}$ orbits are possibly occupied. The occupation of shape driving orbits will increase the probability for the appearance of regular band structure.

The ^{92}Nb nucleus has several valence particles outside the $Z = 38$ submagic and $N = 50$ magic shells and is expected to be spherical. Shell model calculation was carried out to interpret partial structure of ^{92}Nb in this work. A rotational-like band from the 14^- to 20^- states consisting of strong $M1$ and weak crossover $E2$ transitions was observed in ^{92}Nb based on the ^{82}Se(^{14}N, 4n) reaction. An irregular multiplet-like structure is the remarkable feature of nearly spherical nuclei. So it is unusual to observe such a band. The structure indicates weak collectivity and thus a small deformation. With the aim to have a better understanding of the appearance of collectivity in nuclei close to ^{90}Zr, this band is discussed emphatically.

II. EXPERIMENTAL DETAILS

Two reactions were used to construct the level scheme of ^{92}Nb displayed in this work. The first reaction is the ^{14}N + ^{82}Se experiment. High spin states of ^{92}Nb were populated at a beam energy of 54 MeV by the HI-13 tandem accelerator in the China Institute of Atomic Energy (CIAE).

*ljb@jlu.edu.cn
†gxdong@zjhu.edu.cn
‡zgl@buaa.edu.cn

The target consisted of a 0.99 mg/cm^2 layer of ^{82}Se and evaporated on a 8.27 mg/cm^2 thick Yb backing. The γ rays emitted from the reaction residues were detected by a multidetector array consisting of nine Compton-suppressed high-purity germanium (HGPe) detectors and two planar HPGe detectors. The energy resolution of a Compton-suppressed HGPe detector is 2.0–2.5 keV at 1332.5 keV (^{60}Co), and for a planar HPGe detector, it is 0.6–0.7 keV at 121.78 keV (^{152}Eu). These detectors were placed at the forward (40°), 90°, and backward (140°) directions with respect to the beam direction. A total of 1.5×10^8 γ-γ coincidence events were accumulated. The recorded data were sorted into a two-dimensional $E\gamma$-$E\gamma$ symmetric matrix. To obtain multipolarity information of γ rays, two asymmetric coincidence matrices were built, with one axis using the γ rays detected at all angles, and the other using those detected at 40° (or 140°) and those detected at 90°. The gamma ray angular distribution from the oriented nuclei (ADO) ratio is defined as $R_{ADO} = I_\gamma(40^\circ)/I_\gamma(90^\circ)$, which is extracted from the intensity of γ rays observed by detectors at 40° (or 140°) and 90° in the coincidence spectra by setting gates on all detectors. The typical ADO value for stretched quadrupole or $\Delta I = 0$ dipole transitions was found to be 1.4. For stretched pure dipole transitions, it was 0.7.

The second reaction is the ^{6}Li + ^{89}Y experiment. It was performed at the Tandem-XTU accelerator at LNL-INFN in Italy. The target consisted of 550 μg/cm^2 ^{89}Y and was enriched on a 340 μg/cm^2 ^{12}C foil. It was bombarded by the ^{6}Li^{3+} beam at a beam energy of 34 MeV and with an average intensity of 1.0 enA. The gamma rays were detected by the GALILEO array, which is made of 25 Compton-suppressed high-purity germanium (BGO-HPGe) detectors. The detectors were distributed on four rings, ten at 90°, five at each of the following angles, 119°, 129°, and 152°. A two-dimensional $E\gamma$-$E\gamma$ symmetric matrix was constructed for offline analysis. About a total of 1.4×10^7 γ-γ coincidence events were accumulated. The multipolarity information of γ rays was also determined by ADO ratios [$R_{ADO} = I_\gamma(152^\circ)/I_\gamma(90^\circ)$]. The typical ADO value for stretched quadrupole or $\Delta I = 0$ dipole transitions was found to be 1.6. For stretched pure dipole transitions, it was 0.9.

III. EXPERIMENTAL RESULTS

Level structure of ^{92}Nb has been investigated by the direct ^{92}Zr(^{3}He, t) charge-exchange reaction and the ^{88}Sr(^{7}Li, 3n), ^{92}Zr(^{3}He, $p2n$), and ^{92}Zr(p, n) reactions [15–17]. These reactions mainly concentrated on the low-lying states. Recently, some new research results about ^{92}Nb were reported [10,18,19]. It is worth noting that our work is based on the same data with Zheng *et al.* [10] and Lv *et al.* [19]. The ^{82}Se(^{14}N, 4n) reaction was beneficial to populate the high spin states of ^{92}Nb. It has great significance to study a number of interesting nuclear phenomena in high excitation energies. The ^{6}Li^{3+} beam used in our work brings lower excitation energy to the compound nucleus and is in favor of populating the low spin states. It provides opportunity to enrich the level structure with low excitation energy. Almost all transitions between low-energy levels established by Brown and Fossan [15] can be observed by the ^{6}Li + ^{89}Y experiment. However, the 163, 357, and 501 keV transitions in the level scheme were not analyzed completely in Ref. [19].

The result deduced from our work is shown in Fig. 1. Typical prompt γ-γ coincidence spectra are shown in Figs. 2–4. The energies, relative intensities, ADO ratios of γ rays, and spin and parity assignments of levels are summarized in Table I. There are a few points to be noted. Almost all transitions in Ref. [10] are displayed in Fig. 1. Relative intensities of these transitions except the 142, 501, 1444, 1586, and 1945 γ rays can refer to Ref. [10]. For the intensities of the γ rays observed in the ^{6}Li + ^{89}Y experiment and not listed in Table I, see Ref. [19]. That means that data given in Table I are mainly composed of two parts: the first is γ rays which are connected with the 163, 357, and 501 keV transitions and identified by the ^{6}Li + ^{89}Y experiment; the second is new transitions observed by the ^{82}Se(^{14}N, 4n) reaction.

There was a 1507 keV transition decaying from the 1647 to 136 keV level reported in Ref. [16]. However, the energy difference between two levels is 1511 keV. There is no transition observed decaying into the 1648 keV level (which corresponds to the 1647 keV level in Ref. [16]) in our experiment. We could not confirm if there is a linking transition between the two levels.

The structure built on the 357 keV transition and 136 keV level was independent in the scheme of ^{92}Nb in Refs. [15,16]. Several transitions were added which could connect them together. For example, a 1066 keV γ ray can be seen in the spectrum gated on the 501 keV transition as shown in Fig. 2. The 1210 keV transition is found to be coincident with the 357 keV transition. Thus, the level 1567 keV is constructed. Two transitions with energies of 190 and 1020 keV are also observed, whose sum is 1210, which coincide with each other and the 357 keV γ ray. On the spectrum gated on the 190 keV transition, a new transition with energy of 1377 keV is identified. The newly observed 426, 1122, and 1548 keV transitions are assigned to feed on the 357 keV level and lead to the identification of the 1479 and 1905 keV levels. In addition, the 426 keV γ ray is also found to be coincident with the 163 and 1089 keV transitions.

The ^{14}N + ^{82}Se experiment populated the high spin states beneficially. Some linking transitions, such as 742, 1641 keV γ rays, are identified. However, a transition whose energy is above 2605 keV could not be observed based on this data. A 2679 keV transition decaying from the 6005 keV towards the 3326 keV level is found according to the ^{6}Li + ^{89}Y experiment.

IV. DISCUSSION

A. Shell model calculations

Different interactions in the framework of the shell model have been used to interpret the microscopic structure of ^{92}Nb. The GWB model space (which is a standard model space in the shell model code NuShellX [5,23]) without the $h_{11/2}$ orbit has been used in Ref. [10]. However, according to the calculations of several $N = 51$ isotones, the excitation of $d_{5/2}$ neutron across the $N = 56$ subshell closure into the high-j $h_{11/2}$ orbit has great significance [20,21]. So a model space

TABLE I. γ-ray energies, relative intensities, ADO ratios, initial and final E_γ, and initial and final spin states of transitions in ^{92}Nb.

E_γ [a] keV	I_γ [b]	R_{ADO}	E_i keV	E_f keV	J_i^π [c]	J_f^π [c]
89.8(5)	0.90(10)		480	390	4^+	3^-
91	–	–	227	136	2^-	2^+
122.5(3)	6.00(41)	1.28(18)	480	357	4^+	5^+
141.9(2)	3.10(15)	1.81(40)	2087	1945	9^-	7^-
143.3(3)	2.77(22)	0.99(21)	501	357	6^+	5^+
149.6(3)	–	1.00(8)	286	136	3^+	2^+
163.4(2)	18.6(26)	0.99(21)	390	227	3^-	2^-
189.7(3)	1.44(15)	1.50(40)	1567	1377	$(6^+)^*$	$(6^+)^*$
194.0(3)	–	0.97(7)	480	286	4^+	3^+
266.9(4)	1.07(12)	0.82(36)	624	357	$(6^+)^*$	5^+
287.0(4)^a	–	–	7956	7669	–	(17^+)
336.5(3)	0.70(12)	0.77(27)	2514	2177	$(7^+)^*$	$(6^+)^*$
351.1(3)	0.44(6)	1.08(41)	2296	1945	–	7^-
356.7(3)	35.9(28)	1.52(26)	357	0	5^+	7^+
425.5(3)	1.66(17)	0.71(23)	1905	1479	$(6)^*$	$(5^-)^*$
486.1(5)	–	–	2431	1945	–	7^-
500.8(3)	23.82(25)	0.92(17)	501	0	6^+	7^+
569.1(3)	0.45(9)	1.12(36)	2514	1945	$(7^+)^*$	7^-
650.4(4)^a	–	–	11386	10736	–	–
742.0(9)^a	–	–	5683	4941	(15^+)	(15^+)
802.7(5)	–	–	1089	286	–	3^+
861.8(5)^a	–	–	9926	9064	(19^+)	(20^-)
873.4(5)	0.73(10)	–	1374	501	–	6^+
877.4(5)^a	–	–	8781	7904	–	(18^-)
881.4(5)^a	–	–	8514	7633	(19^-)	(17^+)
906.4(7)	3.30(27)	1.02(21)	1407	501	5^+	6^+
919.0(4)	8.41(59)	0.76(14)	1309	390	4^-	3^-
932.3(4)	–	–	1412	480	–	4^+
1019.6(3)	6.79(53)	0.88(19)	1377	357	$(6^+)^*$	5^+
1030.1(6)^a	–	–	9544	8514	–	(19^-)
1031.3(4)	4.41(37)	0.55(15)	1421	390	4^-	3^-
1058.1(6)	–	–	1344	286	–	3^+
1065.7(3)	4.19(33)	1.66(31)	1567	501	$(6^+)^*$	6^+
1089.3(3)	6.0(12)	1.40(30)	1479	390	$(5^-)^*$	3^-
1121.7(4)	5.42(26)	1.42(38)	1479	357	$(5^-)^*$	5^+
1126.2(3)	–	–	1412	286	–	3^+
1129.9(2)	0.80(15)	–	1487	357	–	5^+
1143.9(4)^a	–	–	9926	8781	(19^+)	–
1146.9(4)	1.36(16)	0.45(14)	1648	501	5^+	6^+
1209.7(5)	3.20(29)	–	1567	357	$(6^+)^*$	5^+
1330.9(6)	3.29(33)	1.07(37)	1721	390	$(4^-)^*$	3^-
1377.2(3)	9.9(14)	0.95(40)	1377	0	$(6^+)^*$	7^+
1443.5(3)	6.16(47)	0.97(18)	1945	501	7^-	6^+
1531.0(3)	0.85(13)	–	2032	501	–	6^+
1544.2(6)	–	–	4870	3326	–	13^+
1548.4(4)	1.60(22)	1.07(56)	1905	357	$(6)^*$	5^+
1585.9(4)	3.74(24)	–	2087	501	9^-	6^+
1625.7(6)	2.51(25)	0.71(31)	2127	501	$(7^+)^*$	6^+
1641.0(4)^a	–	–	7324	5683	(17^-)	(15^+)
1769.9(5)	0.98(20)	–	2127	357	$(7^+)^*$	5^+
1819.6(7)	3.64(40)	0.97(35)	2177	357	$(6^+)^*$	5^+
1951.2(8)	3.58(41)	0.88(39)	2308	357	$(6^+)^*$	5^+
2086.9(2)	100	1.40(6)	2087	0	9^-	7^+
2114.8(8)	–	–	5441	3326	–	13^+
2678.9(4)	1.27(16)	–	6005	3326	(16^+)	13^+

[a]Transitions marked with ‘a’ are observed by the ^{14}N + ^{82}Se reaction and information of them comes from the same experiment. Information of the rest γ rays is according to the ^{6}Li + ^{89}Y reaction.

[b]Intensities of transitions are normalized to the 2087 keV γ ray.

[c]J^π labeled with * are determined by ADO ratios measured this time.

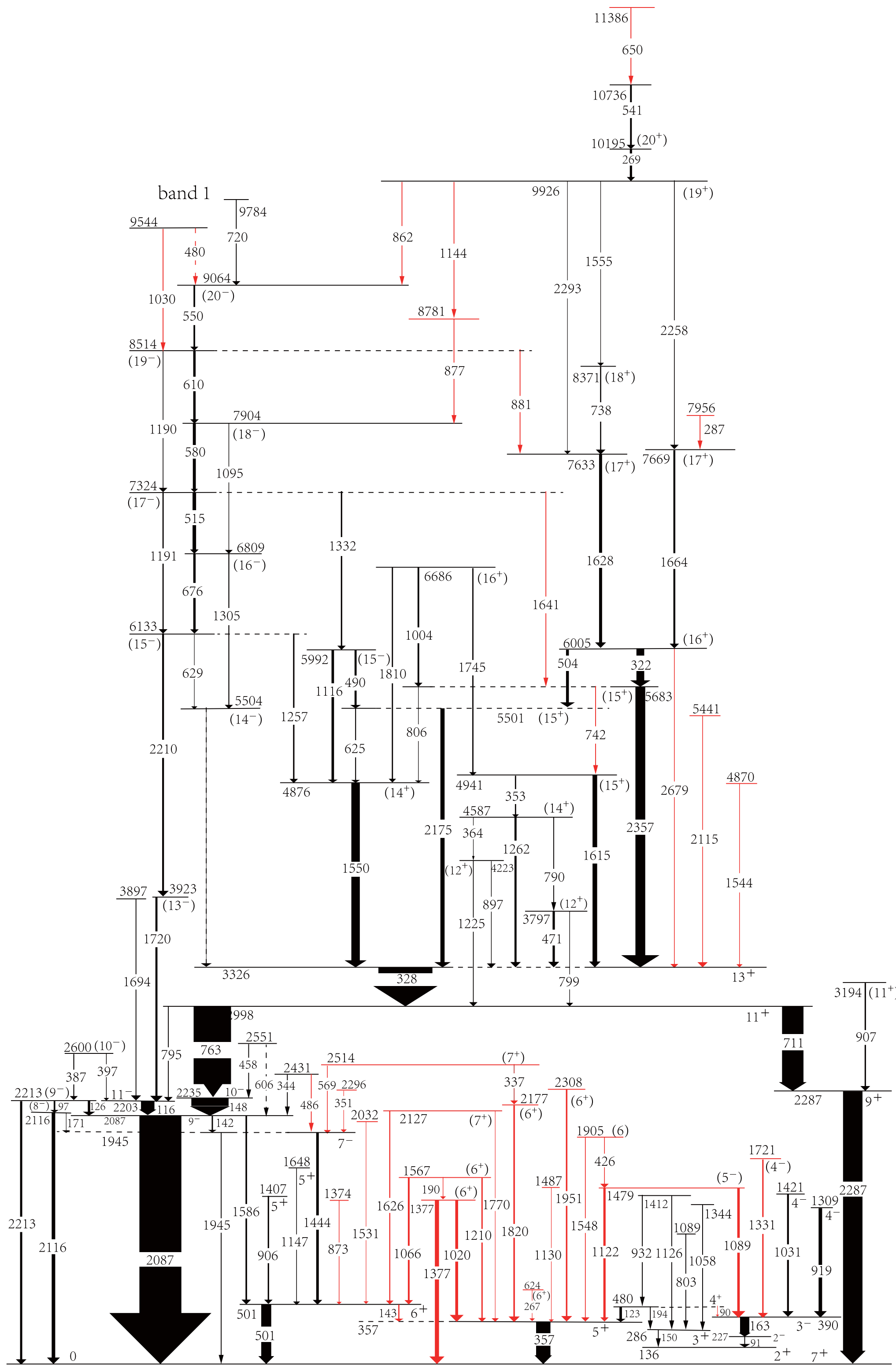

FIG. 1. Level scheme of ^{92}Nb established in the present work. New transitions and levels are marked in red.

named SNE containing the $h_{11/2}$ orbit is adopted. The model space contains eight proton orbits ($f_{5/2}$, $p_{3/2}$, $p_{1/2}$, $g_{9/2}$, $g_{7/2}$, $d_{5/2}$, $d_{3/2}$, $s_{1/2}$) and nine neutron orbits ($f_{5/2}$, $p_{3/2}$, $p_{1/2}$, $g_{9/2}$, $g_{7/2}$, $d_{5/2}$, $d_{3/2}$, $s_{1/2}$, $h_{11/2}$). The corresponding interaction is called the SNET interaction, which is one of the standard interactions available in the NuShellX code [22,23]. Actually, the SNE model space was used in Ref. [19] to interpret the structure of ^{92}Nb, but the authors just calculated the low-lying states. In the present calculation, at most four protons are allowed to excite across the $Z = 38$ subshell. And a neutron at

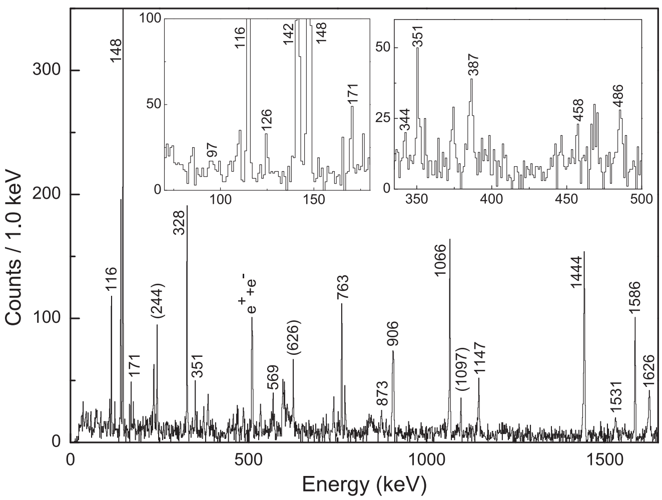

FIG. 2. Spectra gated on the 501 keV transition. Peaks with parentheses are contamination.

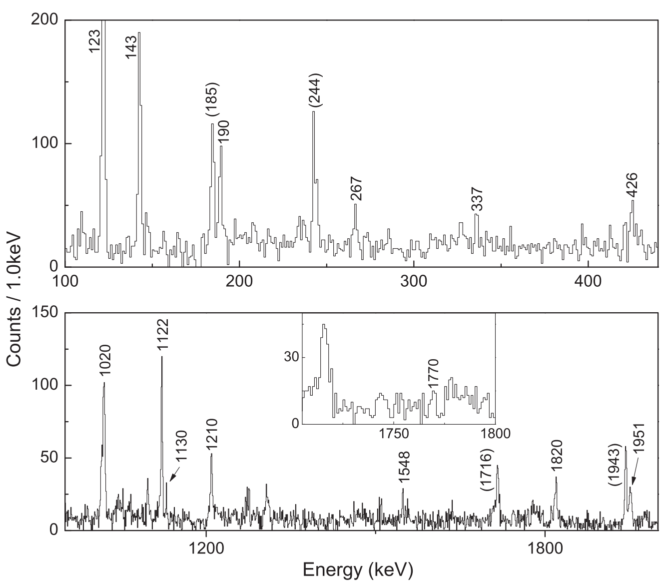

FIG. 3. Spectra gated on the 357 keV transition. Peaks with parentheses are contamination.

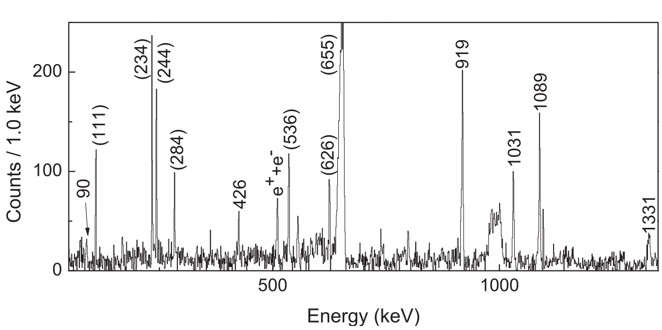

FIG. 4. Spectrum gated on the 163 keV transition. Peaks with parentheses are contamination.

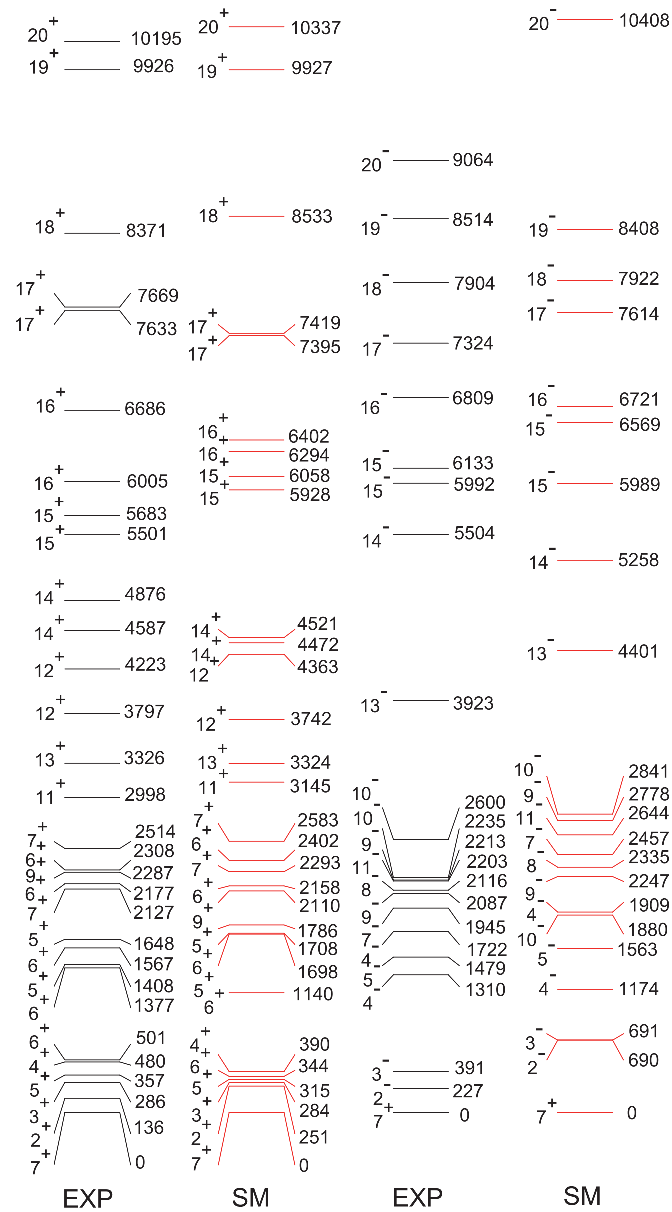

FIG. 5. Comparison of the experimental and calculated energy levels for both positive and negative parity states in ^{92}Nb.

the $g_{9/2}$ orbit is allowed to cross the $N = 50$ shell closure. Comparisons between the experiments and calculations are shown in Fig. 5. The corresponding configurations of the positive and negative parity states are shown in Tables II and III, respectively.

The results reproduce the states up to 14_2^+ well for the positive parity states. Major contribution for these states stems from proton excitations except 14_1^+. The 14_1^+ state is dominated by $\pi[p_{1/2}^1 g_{9/2}^2]\otimes\nu[h_{11/2}]$. The 15^+ state at an energy of 4941 keV is not well reproduced in the calculation, and this state is not included in Table II. The 15_1^+, 16_1^+, 17_1^+, and 18^+ states, at 5501, 6005, 7633, and 8371 keV excitation energies, mainly arise from $\pi[f_{5/2}^5 p_{3/2}^4 p_{1/2}^0 g_{9/2}^4]\otimes\nu[h_{11/2}]$. When it comes to 15_2^+, 16_2^+, 17_2^+, they could be interpreted by the configuration of $\pi[f_{5/2}^5 p_{3/2}^4 p_{1/2}^1 g_{9/2}^3]\otimes\nu[(d_{5/2}/g_{7/2})^1]$. For

TABLE II. Main components of the wave functions and their partitions for the positive parity states in ^{92}Nb. $\pi \otimes \nu$ represents $\pi(f_{5/2}p_{3/2}p_{1/2}g_{9/2}) \otimes \nu(g_{9/2}d_{5/2}g_{7/2}h_{11/2})$.

J^π $\hbar$	$E_{\rm exp}$ keV	$E_{\rm cal}$ keV	Wave function $\pi \otimes \nu$	Partitions
2^+	136	251	6 4 2 1 $\otimes$ 10 1 0 0	31.7%
	–	–	6 4 0 3 $\otimes$ 10 1 0 0	34.7%
3^+	286	284	6 4 2 1 $\otimes$ 10 1 0 0	29.9%
	–	–	6 4 0 3 $\otimes$ 10 1 0 0	36.8%
4^+	480	390	6 4 2 1 $\otimes$ 10 1 0 0	30.7%
	–	–	6 4 0 3 $\otimes$ 10 1 0 0	36.0%
5_1^+	357	315	6 4 2 1 $\otimes$ 10 1 0 0	32.8%
	–	–	6 4 0 3 $\otimes$ 10 1 0 0	36.2%
5_2^+	1407	1698	6 4 0 3 $\otimes$ 10 1 0 0	48.0%
5_3^+	1648	1786	6 4 0 3 $\otimes$ 10 0 1 0	46.1%
6_1^+	501	344	6 4 2 1 $\otimes$ 10 1 0 0	25.5%
	–	–	6 4 0 3 $\otimes$ 10 1 0 0	38.9%
6_2^+	1377	1140	6 4 0 3 $\otimes$ 10 1 0 0	42.5%
6_3^+	1567	1708	6 4 0 3 $\otimes$ 10 0 1 0	46.3%
6_4^+	2177	2158	6 4 2 1 $\otimes$ 10 1 0 0	38.1%
	–	–	6 4 0 3 $\otimes$ 10 1 0 0	24.6%
6_5^+	2308	2402	6 4 0 3 $\otimes$ 10 1 0 0	43.5%
7_1^+	0	0	6 4 2 1 $\otimes$ 10 1 0 0	33.8%
	–	–	6 4 0 3 $\otimes$ 10 1 0 0	34.6%
7_2^+	2127	2293	6 4 0 3 $\otimes$ 10 1 0 0	46.9%
7_3^+	2514	2583	6 4 0 3 $\otimes$ 10 0 1 0	46.7%
9^+	2287	2110	6 4 0 3 $\otimes$ 10 1 0 0	51.2%
11^+	2998	3145	6 4 0 3 $\otimes$ 10 1 0 0	61.3%
12_1^+	3797	3742	6 4 0 3 $\otimes$ 10 1 0 0	64.5%
12_2^+	4223	4363	6 4 0 3 $\otimes$ 10 0 1 0	63.4%
13^+	3326	3324	6 4 0 3 $\otimes$ 10 1 0 0	61.6%
14_1^+	4587	4472	6 4 1 2 $\otimes$ 10 0 0 1	65.0%
14_2^+	4876	4521	6 4 0 3 $\otimes$ 10 0 1 0	53.7%
15_1^+	5501	5928	5 4 0 4 $\otimes$ 10 0 0 1	50.2%
15_2^+	5683	6058	5 4 1 3 $\otimes$ 10 1 0 0	69.0%
16_1^+	6005	6294	5 4 0 4 $\otimes$ 10 0 0 1	44.1%
16_2^+	6686	6402	5 4 1 3 $\otimes$ 10 1 0 0	59.2%
17_1^+	7633	7395	5 4 0 4 $\otimes$ 10 0 0 1	69.4%
17_2^+	7669	7419	5 4 1 3 $\otimes$ 10 0 1 0	75.5%
18^+	8371	8533	5 4 0 4 $\otimes$ 10 0 0 1	69.3%
19^+	9926	9927	4 4 0 5 $\otimes$ 10 1 0 0	69.5%
20^+	10195	10337	4 4 0 5 $\otimes$ 10 0 1 0	71.4%

higher spin states, proton excitation from the *fp* orbits to the $g_{9/2}$ orbit occupies an important position.

For the negative parity states, the difference between the observed 2^- state and the calculated level energy is relatively large, which is 463 keV. The 2^- and 3^- states mainly have the configuration, $\pi[p^1_{1/2}g^2_{9/2}]\otimes\nu[d_{5/2}]$. The 4^-_1, 4^-_2, and 5^- states are predicted to include the excitation of protons across the $Z = 38$ shell. The calculation predicts the involvement of one neutron excitation from the $d_{5/2}$ orbit to the $h_{11/2}$ orbit for the 7^-, 8^-, 9^-_1, and 10^-_1 states, leading to a configuration of $\pi[g^3_{9/2}]\otimes\nu[h_{11/2}]$. While for 9^-_2, 10^-_2, and 11^-, the dominant configuration is $\pi[p^1_{1/2}g^2_{9/2}]\otimes\nu[d_{5/2}]$. The main component in the wave function for the states up to 17^- state is $\pi[f^5_{5/2}p^4_{3/2}p^0_{1/2}g^4_{9/2}]\otimes\nu[(d_{5/2}/g_{7/2})^1]$. The 18^- and 19^- states could be described well by the configuration of

TABLE III. Similar to Table II, but for the negative parity states.

J^π $\hbar$	$E_{\rm exp}$ keV	$E_{\rm cal}$ keV	Wave function $\pi \otimes \nu$	Partitions
2^-	227	690	6 4 1 2 $\otimes$ 10 1 0 0	77.4%
3^-	390	691	6 4 1 2 $\otimes$ 10 1 0 0	71.7%
4_1^-	1309	1174	5 4 2 2 $\otimes$ 10 1 0 0	34.6%
	–	–	5 4 0 4 $\otimes$ 10 1 0 0	22.0%
4_2^-	1721	1909	6 3 2 2 $\otimes$ 10 1 0 0	52.6%
5^-	1479	1563	5 4 2 2 $\otimes$ 10 1 0 0	35.2%
	–	–	5 4 0 4 $\otimes$ 10 1 0 0	21.6%
7^-	1945	2457	6 4 0 3 $\otimes$ 10 0 0 1	37.4%
8^-	2116	2335	6 4 0 3 $\otimes$ 10 0 0 1	39.6%
	–	–	6 4 2 1 $\otimes$ 10 0 0 1	21.6%
9_1^-	2087	2247	6 4 0 3 $\otimes$ 10 0 0 1	43.6%
9_2^-	2213	2778	6 4 1 2 $\otimes$ 10 1 0 0	74.1%
10_1^-	2235	1880	6 4 0 3 $\otimes$ 10 0 0 1	41.5%
	–	–	6 4 2 1 $\otimes$ 10 0 0 1	24.4%
10_2^-	2600	2841	6 4 1 2 $\otimes$ 10 1 0 0	67.7%
11^-	2203	2644	6 4 1 2 $\otimes$ 10 1 0 0	77.1%
13^-	3923	4401	5 4 0 4 $\otimes$ 10 1 0 0	50.2%
	–	–	5 4 2 2 $\otimes$ 10 1 0 0	20.3%
14^-	5504	5258	5 4 0 4 $\otimes$ 10 0 1 0	59.3%
15_1^-	5992	5989	5 4 0 4 $\otimes$ 10 1 0 0	60.5%
15_2^-	6133	6569	5 4 0 4 $\otimes$ 10 0 1 0	65.5%
16^-	6809	6721	5 4 0 4 $\otimes$ 10 0 1 0	56.4%
17^-	7324	7614	5 4 0 4 $\otimes$ 10 1 0 0	49.2%
18^-	7904	7922	5 4 1 3 $\otimes$ 10 0 0 1	76.0%
19^-	8514	8408	5 4 1 3 $\otimes$ 10 0 0 1	75.9%
20^-	9064	10408	4 4 1 4 $\otimes$ 10 0 1 0	73.9%

$\pi[f^5_{5/2}p^4_{3/2}p^1_{1/2}g^3_{9/2}]\otimes\nu[h_{11/2}]$. The 20^- state is not reproduced by the calculation.

Neutron excitations across the $N = 50$ shell gap play an important role in interpreting the structures of nuclei close to ^{90}Zr [1–7]. However, it provides a little contribution to the generation of states with large spin value in our calculation, which is different from Ref. [10]. The same situation occurs in several other $N = 51$ isotones [20,21]. It probably indicates that the excitation of valence neutron across the $N = 56$ subshell closure is easier than the breaking of the $N = 50$ shell. Both mechanisms could bring about large excitation energy to nuclei, as a result, just considering the $N = 50$ inert core excitation is appropriate to describe the level structures. However, referring to calculations for several nuclei with $N > 50$, a large model space including the $h_{11/2}$ orbit is advisable in some cases.

B. Oblate collective rotational band

For nuclei with $N = 51$, with the excitation energy increasing, more protons will be excited to the $g_{9/2}$ orbit. And neutron excitations could not be neglected to interpret the high spin states [1–4,24,25]. There are mainly two kinds of excitation mechanisms: the first is a neutron beyond the $N = 50$ shell excited to the $h_{11/2}$ orbit and the second is neutron excited from the $g_{9/2}$ orbit across the $N = 50$ closed shell to the $d_{5/2}$ orbit. For ^{92}Nb, the ground and low-lying states show the feature of a spherical nucleus and could be described

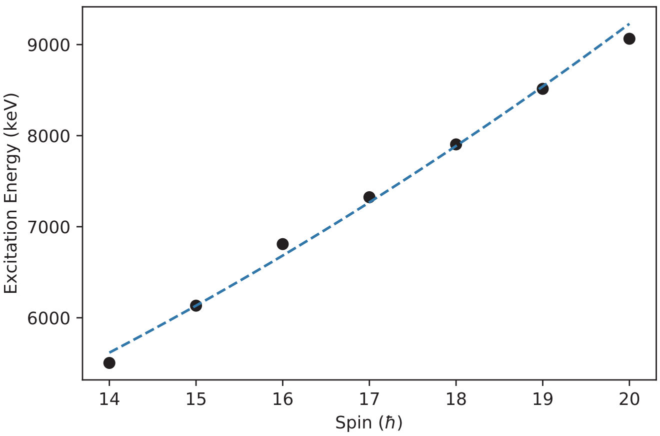

FIG. 6. The excitation energies of states in band 1 have been plotted with the spin values. The blue line is the fitting result to the data using the VMI model.

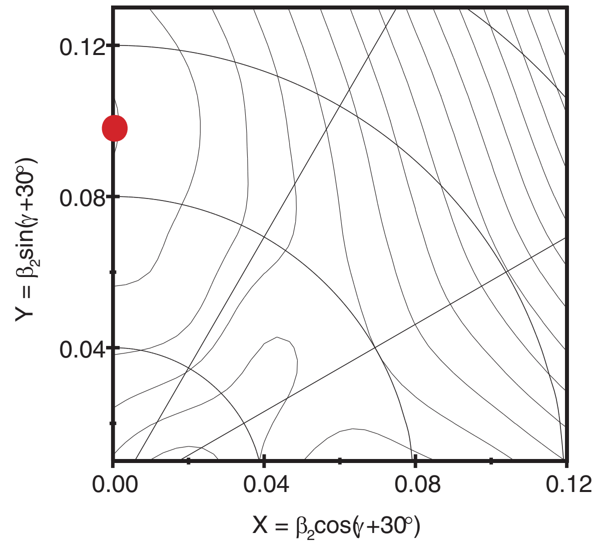

FIG. 7. Configuration constrained potential energy surface for the 14^- state.

well by the shell model. To generate high spin states, the high-j shape driving orbit is occupied, which perhaps drives the nucleus being deformed. The shell model calculation is difficult to apply to the nucleus in this case. The deformation needs to be considered. Consequently, the deviation of the shell model calculations from the experimental data is easily comprehensible.

Using the ^{82}Se(^{14}N, 4n) reaction, the level structure of ^{92}Nb was extended to a higher spin state. It is convenient to research neutron excitations to high-j orbits. A band comprising of enhanced $M1$ transitions with weak crossover $E2$ transitions is observed in the negative parity part, which is marked as band 1 in Fig. 1. The level spacing of the band is relatively regular, resembling a rotational band. In order to test whether the level spacing is regular and to what extent, the variable moment of the inertia model (VMI) is used [26,27]. The model provides the relationship between the excitation energy and angular momentum. Excitation energies of the states in band 1 have been plotted with the spin values labeled as black dots in Fig. 6. The dashed line exhibits the fitting result to the data using the VMI model. The calculated energies reproduced the experiments well and indicates that the structure is relatively regular.

As mentioned, the occupation of high-j shape-driving orbits may induce a weak deformation in the nuclei and leads to the appearance of collectivity at high spin states. With the motivation to test whether deformation occurred and obtain deformation parameters, the potential energy surface calculation using the configuration-constrained method was performed [28]. For a quasiparticle state, the occupied orbitals were fixed and the deformation of a state is determined by minimizing the excitation energies. Potential energy surface was calculated for the 14^- ($\pi[g^3_{9/2}]\otimes\nu[h_{11/2}]$) state. The result is shown in Fig. 7. The deformation parameters are $(\beta_2, \gamma, \beta_4) = (0.098, 60, 0.006)$. It shows that the nucleus has an oblate shape with weak deformation, which is similar to the rotational band observed in ^{93}Nb [14]. In Ref. [29], the ^{90}Mo nucleus was considered to develop an oblate deformation above the 13^+ state due to the occupation of high Ω orbits [413]7/2 and [404]9/2 by a pair of $g_{9/2}$ protons. For the same reason, the ^{92}Nb nucleus shows an oblate deformation. The three $g_{9/2}$ protons occupy the $[440]1/2^+$, $[413]7/2^+$, and $[404]9/2^+$ orbits and the $h_{11/2}$ neutron occupies the high Ω $[505]11/2^-$ orbit. Although the quadrupole deformation is small, it supports our conjecture that deformation occurred and the band 1 is supposed to be an oblate collective rotational band.

A novel kind of nuclear structure phenomena, magnetic rotation, has attracted great interest [30]. It usually corresponds to small quadrupole deformations and is characterized by strong $M1$ transitions with relatively weak or absent $E2$ crossover transitions. The angular momentum is generated by aligning the proton and neutron spin vectors. When it comes to band 1, it shows some features similar to the magnetic rotational band. It is interesting to investigate the origins of the structure. Weak $E2$ transitions can be observed, which manifests weak collectivity and a small nuclear deformation. It conforms to the calculation results nicely. The states of the $M1$ band are generated by a recoupling of the spins of protons and neutrons in high-j orbits. Strong $M1$ and weak $E2$ transitions result in large $B(M1)/B(E2)$ ratios. But it is worth noting that configuration mixing is severe actually under this circumstance, which differs from common rotational bands. It is difficult to find an appropriate model to interpret the band frankly speaking.

V. CONCLUSION

The level scheme of ^{92}Nb has been substantially extended by using the ^{6}Li + ^{89}Y and ^{14}N + ^{82}Se reactions. Spins have been assigned on the basis of the measurement of ADO ratios. Shell model calculations, with the extended model space including the high-j $h_{11/2}$ orbit, give a good description for most states. This indicates the dominant position of single- or multiparticle excitations in ^{92}Nb. However, compared with ruleless structure in most nuclei near ^{90}Zr, a rotational-like band is observed and discussed emphatically. A potential energy surface calculation is performed for the band head. This band shows the characteristic of the oblate collective rotational band due to the occupation of high-j orbits.

ACKNOWLEDGMENTS

This work is supported by the National Nature Science Foundation of China under Grants No. U1867210, No. 11975040, No. U2167204, No. 12275081, and No. U2067205. M.S. is supported by the U.S. Department of Energy, Office of Science, Office of Nuclear Physics, under Contract No. DE-AC02-06CH11357. S.-P.H. is supported by Guangdong Key Research and Development Program No. 2020B040420005, Shenzhen Universities Stable Support Program No. 20200813080048001, and LingChuang Research Project of China National Nuclear Corporation 20221024000072F6-0002-7.

[1] Z. G. Wang, M. L. Liu, Y. H. Zhang *et al.*, Phys. Rev. C **89**, 044308 (2014).
[2] Z. Q. Li, S. Y. Wang, C. Y. Niu *et al.*, Phys. Rev. C **94**, 014315 (2016).
[3] H. Wang, K.-Y. Ma, S.-Y. Liu, and J.-B. Lu, Chin. Phys. C **45**, 094106 (2021).
[4] E. A. Stefanova, R. Schwengner, G. Rainovski *et al.*, Phys. Rev. C **63**, 064315 (2001).
[5] P. Dey, D. Negi, R. Palit *et al.*, Phys. Rev. C **105**, 044307 (2022).
[6] P. W. Luo, X. G. Wu, H. B. Sun *et al.*, Phys. Rev. C **89**, 034318 (2014).
[7] Y.-H. Wu, J.-B. Lu, Z. Ren *et al.*, Phys. Rev. C **105**, 034344 (2022).
[8] M. Bunce, P. H. Regan, V. Werner *et al.*, Phys. Rev. C **87**, 044337 (2013).
[9] E. A. Stefanova, R. Schwengner, J. Reif *et al.*, Phys. Rev. C **62**, 054314 (2000).
[10] Y. Zheng, Y. H. Wu, X. G. Wu *et al.*, Phys. Rev. C **100**, 014325 (2019).
[11] P. Singh, R. Palit, S. Saha, J. Sethi, S. Biswas, D. Choudhury, P. C. Srivastava, and T. Trivedi, Phys. Rev. C **90**, 014306 (2014).
[12] S. Saha, R. Palit, J. Sethi *et al.*, Phys. Rev. C **99**, 054301 (2019).
[13] R Palit and S. Saha, Pramana **82**, 649 (2014).
[14] Y. Wakabayashi, T. Fukuchi, Y. Gono *et al.*, J. Phys. Soc. Jpn. **76**, 114202 (2007).
[15] B. A. Brown and D. B. Fossan, Phys. Rev. C **15**, 2044 (1977).
[16] M. Rumore, C. Fields, and J. Kraushaar, Nucl. Phys. A **445**, 408 (1985).
[17] I. Kumabe, S. Matsuki, S. Nakamura *et al.*, Nucl. Phys. A **218**, 201 (1974).
[18] Y.-H. Wu, J.-B. Lu, P.-W. Luo *et al.*, Chin. Phys. Lett. **31**, 042102 (2014).
[19] Y.-F. Lv, J.-B. Lu, G.-L. Zhang *et al.*, Chin. Phys. C **43**, 104102 (2019).
[20] H. Wang, K.-Y. Ma, Y.-H. Wu *et al.*, Chin. Phys. C **45**, 014001 (2021).
[21] Y. H. Wu, K. Y. Ma, F. Cheng, and X. Y. Cai, Pramana **94**, 53 (2020).
[22] T. Engeland, M. Hjorth-Jensen, and E. Osnes, Nucl. Phys. A **701**, 416 (2002), 5th International Conference on Radioactive Nuclear Beams.
[23] B. Brown and W. Rae, Nucl. Data Sheets **120**, 115 (2014).
[24] S. S. Ghugre, S. Naguleswaran, R. K. Bhowmik, U. Garg, S. B. Patel, W. Reviol, and J. C. Walpe, Phys. Rev. C **51**, 2809 (1995).
[25] E. Galindo, M. Hausmann, A. Jungclaus *et al.*, Phys. Rev. C **69**, 024304 (2004).
[26] M. A. J. Mariscotti, G. Scharff-Goldhaber, and B. Buck, Phys. Rev. **178**, 1864 (1969).
[27] V. Devi and J. S. Matharu, Phys. Scr. **96**, 065309 (2021).
[28] F. Xu, P. Walker, J. Sheikh, and R. Wyss, Phys. Lett. B **435**, 257 (1998).
[29] W. Xiao-Guang, L. Guang-Sheng, P. Zhao-Hua *et al.*, Chin. Phys. Lett. **18**, 505 (2001).
[30] R. M. Clark and A. O. Macchiavelli, Annu. Rev. Nucl. Part. Sci. **50**, 1 (2000).